Investigation of metal doped mesoporous TiO_2 nanostructures for environmental remediation

Santhi K
SRM Institute of Science and Technology
Harish S
SRM Institute of Science and Technology
Navaneethan M
SRM Institute of Science and Technology
S Ponnusamy (suruponnus@gmail.com)
SRM University https://orcid.org/0000-0002-3987-7382

Research Article

Keywords: Nanoparticles, TiO2, visible light, Photocatalysis, Methylene Blue

Posted Date: March 3rd, 2021

DOI: https://doi.org/10.21203/rs.3.rs-261249/v1

Abstract

In the recent past, metal oxides have attracted the researchers because of their applications in energy and environmental application domains. In the present work, hydrothermal technique used to prepared the Sn doped TiO_2 nanoparticles and the effect of Sn concentration has been investigated. The structural, morphological, surface composition, optical and photocatalytic behavior were studied. XRD pattern revealed that doping of Sn makes easy transformation of rutile from anatase phase at lower temperature, providing tetragonal structure of rutile of TiO_2. TEM analysis showed the formation of nanoparticles with spherical like morphology with good crystallinity. UV-Vis spectra, it is observed that optical absorption edge gets red shifted upon Sn doping and the band gap is found to be 2.6 eV. The photocatalytic activity of the synthesized nanoparticles has been investigated under visible light irradiation. Experimental results suggested that 0.5 wt % of Sn doped nanoparticles have shown to exhibit improved photocatalytic properties.

1. Introduction

Water is a precious resource and without it life is not possible on earth. Water is getting polluted day by day due to dyes, organic and inorganic pollutants have become one of the environmental problems which can cause extreme harmful effects to human organisms and appropriate environments [1].

Various methods such as membrane separation, filtration, distillation, adsorption, biological treatment and photodegradation have been developed for the degradation of pollutants through wastewater treatment [2–4]. Among these various methods, photodegradation is found to be the most effective method because of its operational simplicity, complete mineralization and low cost [5–7]. Semiconductor metal oxides such ZnO, CuO, WO_3, NiO, TiO_2, SnO_2 etc., have been widely used owing to its intense catalytic activity and stability. Among these various semiconductors metal oxides utilized, TiO_2 is found to have unique advantages as photocatalysts due to inertness, stability, low operational temperature ,less toxic, significantly low energy consumption and low cost [8]. However, there are few drawbacks for TiO_2 materials to limit their practical application such as wide band gap, high recombination rate and weak separation of charge carriers. These can be avoided by sensitization, doping and coupling of semiconductors [9]. The doping with metal ions and their oxides is one of the most effective methods to extend the absorption in the visible region as well as to enhance the efficiency.

Tin oxide (SnO_2) having a wide band gap (3.8 eV) which exhibits novel properties like unique optical, electronic and catalytic properties. The electronic, ionic and crystallographic properties of SnO_2 are similar to TiO_2 and when coupled with TiO_2 they can easily form substitutional solid solution which not only reduces the band gap but also can provoke in suppression of the charge carrier recombination rate directing to the enhancement of visible light activity [10]. After Sn doping, optical absorption edge shifted to longer wavelength(visible region) [11]. Also Sn can inhibit rutile phase transformation from anatase phase and decrease particle size to enhance the efficiency [12]. Due to large ionic radius of Sn are deposited on the surface of TiO_2 and increases surface area, active site and photocatalytic efficiency [13].

Lin et.al, pridicted that the efficiency nearly 15 times greater than that of anatase TiO_2 while doping Sn [14]. Tu et.al, reported that TIO_2 nanotube arrays have been exihibit optimum dopant amount of Sn is found to be 5.6 wt % [15]. In the present investigation, an attempt has been made to synthesize Sn (up to 0.9 wt %) doped TiO_2 nanoparticles by hydrothermal method and we found optimum dopant amount is 0.5 wt %. The photocatalytic degradation efficiency of the synthesized nanoparticles against Methylene Blue in aqueous solution was studied. It was observed that the increase in Sn doping on TiO_2 represents increase the photocatalytic performance under visible light illumination.

2. Experimental Procedure

2.1 Materials

For synthesis of Sn doped TiO_2 nanoparticles, the precursors, Titanium tetraisopropoxide [$Ti\{OCH(CH_3)_2\}_4$, 98% ; Merck], Tin tetrachloride pentahydrate ($SnCl_4.5H_2O$,, 98% ; Merck), Ammonia (NH_3, 98% ; Merck), Ethanol (C_2H_5OH,, 98% ; Merck) and Methylene blue ($C_{16}H_{18}ClN_3S$,, 99% ; Merck) were purchased from Merck and were used without any further purification.

2.2 Preparation of Sn doped TiO_2 nanostructures:

The sample were prepared by the hydrothermal method. Titanium tetraisopropoxide and Tin tetrachloride pentahydrate were used as a precursor of Ti and Sn, ammonia as surfactant and ethanol as a solvent. 5 mL of Titanium tetraisopropoxide was dissolved in 100 mL of ethanol at room temperature under vigorous stirring for 1h to get complete dissolution. Definite mass of Tin tetrachloride pentahydrates such as 0.1, 0.3, 0.5, 0.7 and 0.9 wt% was dissolved in the exceeding solution and then blend was stirred for 2 h. Then, ammonia was added to the mixture, until solution reaches the pH = 7. Finally, the mixture was placed in a 100 ml of Teflon-lined steel autoclave and maintained 180° C for 24 h. The obtained precipitates washed several times with ethanol and with deionized water by centrifugation and then dried at 80° C for 3 h. The dried samples were annealed at 600° C for 5 h. The resulting samples labeled as ST1 for 0.1% Sn, ST2 for 0.3% Sn, ST3 for 0.5% Sn, ST4 for 0.7% Sn, ST5 for 0.9% Sn and are stored in air – tight container for further studies.

2.3 Characterization

An X' Pert PRO (PANalaytical diffractometer using Kα (λ = 1.5405 Å) radiation at a scan rate of 0.02° / swere used to characterize the crystal structure and phase of the synthesized products. FEI Quanta FEG200 Field Emission Scanning Electron Microscope (FESEM) used to record the images of the prepared samples.. Transmission Electron Microscopy (TEM) micrograph were recorded using a JEOL JEM 2100F microscopeat an accelerating voltage of 200 kV. Functional group analysis was carried out by Bruker IFS 88 Fourier Transform InFrared (FTIR) spectrometer equipped with a MCT cryodetector. Optical absorption studies were done by shimadzu UV-2600 spectrophotometer. X-ray Photoelectron Spectra (XPS) were measured by Shimadzu ESCA 3400. Raman spectra were done with JASCO NR-1800 spectrometer. Photoluminescence spectra recorded with Model S4 PIONEER BRUKER spectrometer.

2.4 Photocatalytic measurement

Sn doped TiO_2 nanoparticles were tested against methylene blue (MB) dye in aqueous solution for photocatalytic activities. The degradation experiment was studied by implementingimmersion type photo reactor with container have quartz tube. Photocatalytic activity was carried out using 150 W (Heber scientific suppliers) tungsten lamp at wavelength greater than 400 nm and the irradiation intensity measured by lux meter was 23000 1ux. The MB dye solution (100 mL; 3 ppm) were prepared. UV-visible spectrometer used to record the absorption spectrum shows the maximum absorption intensity at 664 nm Then, 10 mg of synthesized sample was added to the MB dye solution and the solution wascontinuously stirred for 10 min in dark condition to analyze adsorption and desorption equilibrium between catalystand MB dye. The visible light used to irradiated with stable aqueous dye solution for 10 min and at every 10 min interval, the UV absorption spectra was recorded and continued upto 30 min at the end of the cycle, the solution was centrifuged to separate TiO_2 particles. The following Eq. (1) used to calculate thephotodegradation percentage of MB[16].

$$D\,(\%) = \left[\frac{1 - C_t}{C_0}\right] \times 100$$

1

where $C_0$is the initial concentration of the dye solution and C_t is the concentration of the dye solution at every 30 min interval during the photocatalytic reaction.

3. Results And Discussion

The crystal structure and phase of the Sn doped TiO_2 nanoparticles (ST1, ST2, ST3, ST4, ST5) were determined by XRD (Fig. 1(a)). The peaks at 27.08°, 34.45°, 38.47°, 52.40°, 55.24°, 62.56°, 65.56°, 66.50° for sample ST5 were assigned to (110),(101),(200),(211),(220),(002), (301),(112) lattice planes of the tetragonal structure of rutile TiO_2. These values are well matched with JCPDS card no (21-1276) [17]. The peaks obtained at 2θ values 25.3°, 37.8°, 48.1°, 53.9°, 55.1°, 62.8°, 68.8° 70.8° and 75.1° corresponds to (101), (004), (200), (105), (211), (204), (116), (220) and (215) crystal planes indicating the formation of tetragonal structure of anatase phase TiO_2 nanopowders shown in Fig. 1(d) (JCPDS Card No 21-1272) [18]. Here we report that formation of only rutile phase and higher crystallinity due to Sn doping. The dominant peaks are observed at 27.08°, 34.45°, 38.47°, 52.40°, 58.58° were assigned to (110),(101),(200), (211),(301) lattice planes of the tetragonal structure rutile SnO_2. The observed values are well matched with JCPDS card no (41-1445) [19]. It was interesting to found that TiO_2 and SnO_2 oxides be the possession of the same crystal symmetry (Tetragonal) [20]. The sample ST5 slightly shift to the lower angle (0.79°) when compared with ST1.

Figure 1(b) is the extended view of XRD. It shows the diffraction peak slightly move to a lower angle with increasing Sn content. The ionic radius and electronegativity of the Sn^{4+} ion are near to the Ti^{4+} ion [12,

21, 22]. When the Sn content increases Sn^{4+} (0.0071 nm) occupy the lattice position of Ti^{4+} (0.0068 nm) due to large ionic radius. As a result, the interplanar distance increases from 0.3200 nm to 0.3290 nm calculated from Braggs equation. This confirms the size increases after Sn doping. Moreover, in all the samples, Sn peak is not appeared in the XRD pattern. It is concluded that the Sn^{4+} ion has been successfully incorporated into the crystal lattice site of Ti^{4+} [23, 24]. Scherrer formula used to calculate the crystallite size for predominant peak which corresponds to the plane (110). For ST1 sample, it was found to be 18.5 nm. Meanwhile, the amount of Sn in the synthesized samples increases the crystallite size from 13.8 nm to 9 nm decreases for the sample ST1 to ST3 which was confirmed by other researchers [25]. The crystallite sizes decrease gradually upto 0.5 wt% Sn doping and then increases for 0.7 wt% and 0.9 wt% of Sn due to ionic radius and enhanced agglomeration. Substitution of large sized Sn^{4+} in Ti^{4+} to the introduction of oxygen vacancies as a result in an increase photocatalytic efficiency. In general, the larger the surface area, smaller crystallite size to induce the separation of charge carriers and photocatalytic efficiency. Figure 1(c) shows the particle size with different concentration. The calculated XRD parameters of the prepared samples specified in Table 1.

Figure 2 shows the Raman spectra of Sn doped TiO_2 nanoparticles. There are three Raman active modes are well observed at 143 cm^{-1},443 $cm^{-1}$and 610 cm^{-1}, respectively. These modes are attributed to the B_{1g} band, due to symmetric bending vibration of O-Ti-O, E_g band is due to symmetric stretching vibration of O-Ti-O and A_{1g} band is due to antisymmetric bending vibration of O-Ti-O in TiO_2 respectively [26]. The peak at 237 cm^{-1} and 320 cm^{-1} is strong second-order or disorder induced Raman scattering [27, 28], which is a result of multi-phonon processes. The peak at 143 $cm^{-1}$and 320 cm^{-1} disappear due to higher concentration of Sn. Which was good agreement with XRD results. Moreover, all the samples preserved the rutile structure which suggest that Sn dopant are substitutionally incorporated in TiO_2 lattice [29]. When concentration of Sn increases in TiO_2 lattice the peak shift in *Eg* mode from 443 cm^{-1} to 430 cm^{-1} and A_{1g} mode from 610 cm^{-1} to 628 cm^{-1} were observed. The shift in raman peak occur due to high lattice defect such as oxygen vacancies can be created by doping of Sn ions [30, 31].

The morphological analyses of Sn doped TiO_2 nanoparticles were performed by FESEM, TEM and HRTEM as shown in Fig. 3. The FESEM images for the sample ST1 [3(1(a))] and sample ST2 [3(2(a))] shows the mesoporous assembly, composed of rough spherical nanaoparticles, which are clustered and agglomerated. The particle size as measured through image is found to be 18 – 13 nm. The increasing content of Sn influences the particle size and cluster formation as depicted in [Fig. 3(3(a))]. It seen that for higher concentration of Sn the cluster formation gets distorted and the particle size from 9 nm to 15 nm increased due to larger ionic radius of Sn as shown in [Fig. 3(4(a))] and [Fig. 3(5(a))] [32, 33, 34]. TEM images of the samples shown in [Fig. 3(1(b))] to [Fig. 3(5(b))] reveals that the particles are agglomerated with size of about 8 nm 20 nm [35, 36]. From the HRTEM images [Fig. 3(1(c))] to [Fig. 3(5(c))], it apparent that the particle consists of uniform and highly crystalline. The uniform fringes with lattice spacing of 0.32 nm corresponding to (110) rutile phase is observed. The lattice fringes spacing increase from 0.3200 nm to 0.3290 nm and shows considerable waviness. The expansion of fringes is caused by the defects

possibly due to electric stress that may exist from Sn doping in TiO_2 matrix [37]. From the above morphological analysis, possible growth mechanism explained as shown in Pattern I.

FTIR spectra for the samples were recorded and are used to identify the functional groups and chemical bonding in TiO_2 and SnO_2 nanoparticles in the range of 400 cm^{-1} to 4000 cm^{-1} The peak at 2339 cm^{-1} can be assigned to *C-H* vibrational band due to source of titanium.[38]. The peak at 3665 cm^{-1}attributed to stretching vibration of *O-H* molecule. The peak at 432 cm^{-1} nominate to stretching vibration modes of *Ti-O* bonds and 800 cm^{-1} attributed to stretching vibration modes of *Sn-O* in prepared samples. The presence of *Sn-O* bond demonstrates that successful incorporation of SnO_2 nanoparticles in TiO_2 lattice [39].

The optical absorption of the samples shown in Fig. 5(a). The dopant energy level (sub bands) formed within the forbidden gap of TiO_2 lattice after Sn doping. Due to that absorption edges of the prepared samples are red shifted from 425 nm to 520 nm. The red shift ensures the charge transfer between Sn^{4+} electron and the conduction band of TiO_2 [40, 41]. It clearly mention the energy band gap decreases and improve the photocatalytic efficiency. The band gap energy of the prepared samples was calculated using the Tauc plot. The Tauc's equation is given by

$$(\alpha h\upsilon) = A(h\upsilon - E_g)^n$$

2

where *a, v, A* and E_g are the absorption coefficient frequency, proportionality constant and band gap energy respectively. In above equation n = 2 is a constant for direct transition [42, 43]. The calculated band energy decreased from 2.90 eV to 2.61 eV as the content of Sn increases from 0.1 to 0.9 wt% as shown in Fig. 5(b).

XPS spectra are presented in Fig.6. Figure 6(a) shows the Ti 2p states of TiO_2 consists of two peaks Ti $2p_{3/2}$ and Ti $2p_{1/2.}$ The Ti $2p_{3/2}$ peaks for samples ST1, ST2, ST3, ST4 and ST5 are observed at 459.4 eV, 459.2 eV, 459.1 eV, 459.1 eV and 459 eV respectively. Ti $2P_{1/2}$ peaks for samples ST1, ST2, ST3, ST4 and ST5 are observed at 465.2 eV, 465.1 eV, 464.9 eV, 464.9 eV and 464.7 eV, respectively. It can clearly observe that binding energy for Ti $2p_{3/2}$ increased by 0.4 eV and Ti $2p_{1/2}$ increased by 0.5 eV towards higher binding energy. This shift is confirmed by formation of Ti^{4+} and O–Ti–O and Ti–O–Sn, which corresponds to Ti $2p_{3/2}$ and Ti $2p_{1/2}$ respectively [**44**]. The electron density (number of electron) of rutile TiO_2 increase while doping Sn [**45,46]**. The splitting between Ti $2p_{1/2}$ and Ti $2p_{3/2}$ was 5.7 eV, indicate Ti $^{4+}$ state in the Sn doped TiO_2 nanoparticles. The addition of Sn $^{4+}$ is responsible for shift in binding energy of Ti $2p_{3/2}$ and Ti $2p_{1/2}$ compared to the reported value [**47, 48**]. 0.4 eV shift observed in Ti $2p_{3/2}$ and 0.5 eV shift observed in Ti $2p_{1/2}$. The substitution of Sn into Ti lattice directing to the binding energy shift due to electronegativity of Sn is larger than that of Ti. The work function of SnO_2 and TiO_2 is 4.4 eV and 4.2 eV, electron affinity is 4.7 eV and 4.2 eV [49**, 50**]. For Sn 3d (Figure 6(b)) the peak at 487.1eV and 495.5 eV was assigned for Sn $3d_{5/2}$ and Sn 3d $_{3/2}$ respectively, and the splitting of the 3d doublet of Sn is 8.4 eV,

and also small shift (0.2 eV) observed. This indicated a valence state of Sn $^{4+}$ [**51, 52**]. XPS spectra of O 1s level shown in Figures 6 (c (1)) – 6 (c (5)). It can clearly observe that O 1s consists of peak at 530.8 eV which are produced by lattice oxygen (O_L) in Ti-O-Ti bonds [**53, 54**] and 532.1 eV can be attributed to the hydroxyl group (O_H) [**55**].

The recombination probability for prepared photocatalyst was characterized by photoluminescence spectroscopy. Figure 7 shows that 385 nm 400 nm were assigned to the band to band PL emission which was created by incident light energy which is approximately equal to that of band gap of the rutile phases of TiO_2 respectively [56, 57]. The excitonic peak at 436 nm is assigned to defect in TiO_2 nanoparticles [58]. The PL peak located at the 526 nm is related with the shallow trap on surface oxygen vacancies of TiO_2 [59]. It has been clearly found that the PL intensity decreases from sample ST1 to ST3 with increasing Sn content in TiO_2 because of generated electron-hole pair can affect the charge transfer between the interface of Sn and TiO_2 resulting recombination rate is reduced. The decreasing charge carrier recombination rate is suitable for increasing photocatalytic activity. The PL spectra demonstrate a slight red shift. Which is in good agreement with UV spectra [60]. As the concentration of Sn increases, the PL intensity increases for samples ST4 and ST5, because the trap electrons increase the recombination rate, decreases the photocatalytic activity.

3.1 Photocatalytic activities of Sn doped TiO_2 nanoparticles:

The photocatalytic behavior of the synthesized nanoparticles was studied against methylene blue (MB) under visible light irradiation and the results are displayed in Fig. 8. Figure 8 (a) shows the time-dependent UV-visible absorption spectra of the MB solution in the presence of ST3 sample. The highest degradation efficiency is found to be 95.3% (Initial dye concentration = 3 ppm/L,Catalyst loading = 10 mg/L, Time = 30 minutes). Effect of Sn on the photodegradation efficiency of MB under visible light is shown in Fig. 8(b). Increase in Sn dopant concentration to 0.5% increases the photocatalytic activity and reaches maximum. Loading of Sn on TiO_2 can greatly inhibit the charge carriers recombination and enhances the photocatalytic efficiency. Although, SnO_2 and TiO_2 are reported to be wide band gap semiconductors, the band gap of SnO_2 (3.8 eV) is wider than that of rutile TiO_2 (3.0 eV) and the Fermi level of SnO_2 is lower than that of TiO_2 [61]. Since, the dopant energy level of Sn lies very close to conduction band of TiO_2, the photogenerated electrons can be readily transferred from TiO_2 to the Sn doping energy level. With increase in Sn doping more photogenerated electrons are transferred to the surface under illumination. Addition of Sn on TiO_2 not only suppresses the recombination of photogenerated electrons and holes, but also increases the degree of light absorbance to generate electrons because of the decreasing band gap. Thus increase of Sn dopant concentration can act as efficient electron traps, promoting the separation of photogenerated electron- hole pairs and reducing the degree of their recombination, leading to the enhancement of photocatalytic activity. Further increase in Sn amount results in decreased active surface area on the TiO_2 surface thereby reducing the amount of adsorbed active-OH groups on the surface of TiO2. Hence at higher concentration of Sn the efficiency of photocatalytic activity decreased.

However, there exists an optimal amount of dopant. Here we report optimal value of dopant is 0.5%. Below the optimal value of Sn dopant, the photocatalytic activity increases, but higher than optimal value the photocatalytic activity decreases due to average distance between the trap sites decreases [62].

The degradation percentage is calculated to be 93.5 % for STT1, 87.9 % for ST2, 95.3 % for ST3,93.1 % for ST4 and 86.4 % for ST5 respectively. The comparison was made between the photocatalytic decomposition performed in this work and other reported work as shown in Table 3.

Figure 8 (c) shows that photdegradation of MB solution for different photocatalyst. The photocatalytic activity was studied using Lagmuir-Hinshelwood kinetics model [63]. Figure 8 (d) shows that kinetic curve of photocatalytic degradation of MB with different catalyst. The degradation of MB under visible light obeyed the pseudo-first order reaction kinetics as follows.

$$\ln\left[\frac{C_0}{C_t}\right] = K_{obs}t \,(3)$$

where C_0 is the initial concentration of the dye solution and C_t is the concentration of the dye solution at every 10 min and K_{obs} is the apparent rate constant. The values for the degradation rate constant are shown in Table 2.

3.2 The Plausible photocatalytic mechanism of Sn doped TiO_2 nanoparticles

The Plausible photocatalytic mechanism of prepared nanoparticles towards the degradation of MB under visible light is demonstrate in Fig. 9. The Fermi energy level of TiO_2 is grater than that of SnO_2 due to its smaller work function so electron transfer occurs from TiO_2 to SnO_2 and hole transfer from SnO_2 to TiO_2 [64]. When sample is irradiated with visible light the electron in the valance band (VB) get excited to the conduction band (CB). The holes were created in the valance band. Thereafter the electron and holes were transferred to the surface of the crystal and react with the molecular oxygen (O_2) and H_2O for generating the super oxide radical anion ($^{\bullet}O_2^-$) and hydroxyl radicals ($OH^{\bullet}$). The possible mechanism of photocatalytic reactions of MB dye as follows

$Zn - TiO_2 semicondutorphotocatalyst + hv \rightarrow h^+ + e^-$ (4)

$Semiconductor\ h^+ + H_2O \rightarrow OH^{\bullet} + Semiconductor\ H^+$ (5)

$Semiconductor\ h^+ + OH^- \rightarrow OH^{\bullet}$ (6)

$Semiconductor\ h^+ + \text{Dye} \rightarrow Oxidation\ products$ (7)

$O_2 + Semiconductor\ e^- \rightarrow {}^{\bullet}O_2^-$ (8)

${}^{\bullet}O_2^- + 2H^+ \rightarrow H_2O_2$ (9)

Semiconductor $e^- + H_2O_2 \rightarrow OH^{\bullet}$ (10)

Dye + *Semiconductor* $e^- \rightarrow$ *Reduction products* (11)

$OH^{\bullet}$ +Dye (MB) + $O_2 \rightarrow CO_2 + H_2O$ + Other degradation products. **(12)**

3.3. Reusability:

The stability and reproducibility of the photocatalyst are very important. Hence, the photocatalyst was monitored by repeating the reaction procedure. At the end of the each reaction, the photocatalyst was cleaned using ethanol and distilled water to get precipitate. Then dried in hot air oven 80 °C for 1 h to reuse for the next reaction. The degradation rate was detected at 95.3% for first time, second time slightly decreased to 93.7% and third time 93.2%. This clearly shoes that ST3 have better stability. After the third cycle was not able to collect the sample.

4. Conclusion

In the current work, Sn doped TiO_2 nanoparticles prepared by hydrothermal method. From the XRD results the diffraction angle slightly shift to lower angle which confirms the Sn present in the TiO_2 lattice. Optical spectra confirm the decreases in energy band gap as the Sn content increases. These parameters direct to the conclusion, an appropriate amount of Sn to enhance the efficiency. The optimum dopant amount of Sn is found to 0.5% in our experiment. It was concluded that Sn doped TiO_2 nanoparticle (ST3) shows the highest degradation efficiency (95.3%). The novelty of this work was by using less quantity of photocatalyst we obtained better photocatalytic activity when compare to other reported work.

References

1. Z.Y. Zhang, C.L. Shao, X.H. Li, L. Zhang, H.M. Xue, C.H. Wang, Y.C. Liu, Electrospun nanofibers of ZnO-SnO_2 heterojunction with high photocatalytic activity. J. Phys. Chem. C **114**, 7920–7925 (2010)
2. G. Yang, T. Wang, B. Yang, Z. Yan, S. Ding, T. Xiao, Enhanced visible-light activity of F-N co-doped TiO_2 nanocrystals via nonmetal impurity, Ti^{3+} ions and oxygen vacancies. Appl. Surf. Sci. **287**, 135–142 (2013)
3. S. Pitchaimuthu, S. Rajalakshmi, Enhancement of zinc oxide-mediated solar light decoloration of Acid Yellow 99 dye by addition of b -CD. Appl. Water Sci. **2**, 201–208 (2014)
4. G. Zhao, L. Liu, J. Li, Q. Liu, Efficient removal of dye MB: through the combined action of adsorption and photodegradation from $NiFe_2O_4/Ag_3PO_4$. J. Alloy. Compd. **664**, 169–174 (2016)
5. S.M. El-Dafrawy, M. Farag, S. Abd, E. Hakam, S.M. Hassan, Structural and catalytic properties of sulphated zirconia doped by Zn oxide. Egypt. J. Chem. **345**, 329–345 (2017)
6. A.H. Hattab, A.I. Ahmed, S.M. Hassan, A.A. Ibrahim, Photocatalytic degradation of methylene blue by modified nanoparticles titania catalysts. Int. J. Mod. Chem. **7**, 45–53 (2015)

7. S.M. El-Dafrawy, M. Farag, S.M. Hassan, Photodegradation of organic compounds using chromium oxide-doped nano-sulfated zirconia. Res. Chem. Intermed. **43**, 6343–6365 (2017)
8. M. Pelaeza, N.T. Nolanb, S.C. Pillai, M.K. Seeryc, P. Falarasd, D.D. Dionysiou et al., A review on the visible light active titanium dioxide photocatalysts for environmental application. Appl. Catal., B **125**, 331–349 (2012)
9. L. Pan, J.-J. Zou, X. Zhang, L. Wang, Water-Mediated Promotion of Dye Sensitization of TiO_2 under Visible Light. J. Am. Chem. Soc. **133**, 10000–10002 (2011)
10. O. Carp, C.L. Huisman, A. Reller, Photoinduced reactivity of titanium dioxide. Prog. Solid State Chem. **32**, 33–177 (2004)
11. M. Huang, J. Yu, B. Li, Ch Deng, L. Wang, W. Wu, L. Dong, F. Zhang, M. Fan, Intergrowth and coexistence of TiO_2-SnO_2 nanocomposite with excellent photocatalytic activity. J. Alloy. Comp. **629**, 55–61 (2015)
12. K. Rubenis, J.Locs,J. Mironova, R.M. Meri, Influence of phase separation on thermal conductivity of $Ti_{1-x}Sn_xO_2$ Ceramics, J. Ceram. Sci. Tech.,07[01], 135–138 (2016)
13. N. Kiraz, E. Burunkaya, O. Kesmez, H.E. Camurlu, M. Asilturk, ,Z. Yesil, E. Arpa, Preparation of Sn doped nanometric TiO_2 powders by reflux and hydrothermal syntheses and their characterization. J. Sol-Gel Sci.Tech. **59**, 381–386 (2011)
14. J. Lin, J.C. Yu, D. Lo, S.K. Lam, Photocatalytic Activity of Rutile $Ti_{1-x}Sn_xO_2$. Solid Solutions J. Catal. **183**, 368–372 (1999)
15. Y.F. Tu, S. Huang, J.P. Sang, X.W. Zou, Synthesis and photocatalytic properties of Sn- doped TiO_2 nanotube arrays. J. Alloys Compd. **482**, 382–387 (2009)
16. R. Sankar Ganesh, S.K. Sharma, E. Durgadevi, M. Navaneethan, S. Ponnusamy, C. Muthamizhchelvan, Y. Hayakawa, Deuk Young Kim, Growth, microstructure, structural and optical properties of PVP-capped CdS nanoflowers for efficient photocatalytic activity of Rhodamine B. Mater. Res. Bull. **94**, 190–198 (2017)
17. F.Z. Haque, R. Nandanwar, P. Singh, Evaluating photodegradation properties of anatase and rutile TiO_2 nanoparticles for organic compounds. Optik **128**, 191–200 (2017)
18. K. Santhi, M. Navaneethan, S. Harish, S. Ponnusamy, C. Muthamizhchelvan, Synthesis And Characterization Of TiO_2 Nanorods By Hydrothermal Method With Different pH Conditions And Their Photocatalytic Activity. Appl. Surf. Sci. **500**, 144058 (2020)
19. R.N. Mariammal, K. Ramachandran, B. Renganathan, D. Sastikumar, On the enhancement of ethanol sensing by CuO modified SnO_2 nanoparticles using fiber-optic sensor. Sensors and Actuators B **169**, 199–207 (2012)
20. Y. Cao, T. He, L. Zhao, E. Wang, W. Yang, Y. Cao, Structure and phase transition behavior of Sn^{4+} Doped TiO_2 nanoparticles. J. Phys. Chem. C **113**, 18121–18124 (2019)
21. C.W. Soo, C.W. Lai, G.T. Pan, T.C.K. Yang, K.M. Lee, R.M. Yusop, J.C. Juan, Effects of various hydrogenated temperatures on photocatalytic activity of mesoporous Titanium dioxide. Micro & Nano

Letters **13**(1), 77–82 (2018)

22. Y. Cao, T. He, Y. Chen, Y. Cao, Fabrication of Rutile TiO_2- Sn/Anatase TiO_2-N Heterostructure and its application in visible light photocatalysis. J. Phys. Chem. C **114**, 3627–3633 (2010)
23. J. Li, X. Xu, X. Liu, C. Yu, D. Yan, Z. Sun, Likun Pan, Sn doped TiO_2 nanotube with oxygen vacancy for highly efficient visible lightphotocatalysis,, *J. Alloys Compd.* (2016)
24. D.A. Solis-Casados, L. Escobar- Alarcon, L.M. Gomez- Olivan, E. Haro-Poniatowski, T. Klimova, Photodagradation of pharmaceutical drugs using Sn-modified TiO_2 powders under visible light irradiation, Fuel (2017)
25. M. Manzoor, A. Rafiq, M. Ikram, M. Nafees, S. Ali, Structural, optical, and magnetic study of Nidoped TiO_2 nanoparticles synthesized by sol–gel method. International Nano Letters **8**, 1–8 (2018)
26. I. Singh, Balaji Birajda, Synthesis, characterization and photocatalyticactivity of mesoporous Na-doped TiO_2 nano-powder prepared via a solvent-controlled non-aqueous sol–gel route. RSC Adv. **7**, 54053–54062 (2017)
27. X. Tian Lan, Tang, B. Fultz, Phonon anharmonicity of rutile TiO_2 studied by Raman spectrometry and molecular dynamics simulations. Phys. Rev. B **85**, 094305 (2012)
28. U.Balachandran and N.G.Eror, Raman spectra of Titanium Dioxide. J. Solid State Chem. **42**, 276–282 (1982)
29. T. Ali, A. Ahmed, U. Alam, I. Uddin, P. Tripathi, M. Muneer, Enhanced photocatalytic and antibacterial activities of Ag-doped TiO_2 nanoparticles under visible light. Mater. Chem. Phys. **212**, 325–335 (2018)
30. Y. Wang, K. Nomura, X. Liu, A.I. Rykov, C. Jin, T. Liu, J. Wang, Structural and Magnetic Properties of 57Fe-Doped TiO_2 and 57Fe/Sn-Codoped TiO_2 Prepared by a Soft-Chemical Process, Eur. J. Inorg. Chem. 2131–2135 (2016)
31. Y. Wang, Y. Zhang, F. Yu, C. Jin, X. Liu, J. Ma, Y. Wang, Y. Huang, J. Wang, Correlation investigation on the visible-light-driven photocatalytic activity and coordination structure of rutile Sn-Fe-TiO_2 nanocrystallites for methylene blue degradation. Catal. Today **258**, 112–119 (2015)
32. A. Arunachalam, S. Dhanapandian, C. Manoharan, Effect of Sn doping on the structural, optical and electrical properties of TiO_2 films prepared by spray pyrolysis. J. Mater. Sci.: Mater. Electron. **27**, 659–676 (2016)
33. S.M. Hassan, A.I. Ahmed, M.A. Mannaa, Structural, photocatalytic, biological and catalytic properties of SnO_2/TiO_2nanoparticles. Ceram. Int. **44**, 6201–6211 (2018)
34. M. Huang, S. Yu, B. Lin, L. Dongn, F. Zhang, M. Fan, L. Wang, J. Yu, C. Deng, Influence of preparation methods on the structure and catalyticperformance of SnO_2-doped TiO_2 photocatalysts. Ceram. Int. **40**, 13305–13312 (2014)
35. H.A. Alhadrami, A. Baqasi, J. Iqbal, R.A.M. Shoudri, A.M. Ashshi, E.I. Azhar, F. Al-Hazmi, A. Al-Ghamdi, S. Wageh, Antibacterial Applications of Anatase TiO_2 Nanoparticle. American Journal of Nanomaterials **5**, 31–42 (2017)

36. C.M. Magdalane, K.M.V. Arularasu, G. Ramalingam, K.Kaviyarasu,Self-cleaning mechanism of synthesized SnO_2/ TiO_2 nanostructure for photocatalytic application for waste water treatment. Surf. Interfaces. **17**, 100346 (2019)
37. X. Zhu, L. Pei, R. Zhu, Y. Jiao, R. Tang, W. Feng, Preparation and characterization of Sn/La co-doped TiO_2 nanomaterials and their phase transformation and photocatalytic activity. Sci. Rep. **8**, 12387 (2018)
38. S. Fereshteh Akhtari, M. Zorriasatein, Farahmandjou, S.M. Elahi, Synthesis and optical properties of Co^{2+}-doped ZnO Network prepared by new precursors. Mater. Res. Express **5**, 065015 (2018)
39. S. Ehsan, H. Yeganeh, M. Kazazi, B.K. Kaleji, S.H. Kazemi, B. Hosseinzadeh, Electrophoretic deposition of Sn-doped TiO_2 nanoparticles and its optical and photocatalytic properties. J. Mater. Sci.: Mater. Electron. **29**, 10841–10852 (2018)
40. X. Li, R. Xiong, G. Wei, Preparation and photocatalytic activity of nanoglued Sn-doped TiO_2 J. Hazard. Mater. **164**(2–3), 587–591 (2009)
41. R. Nirmala, H.Y. Kim, R. Navamathavan, C. Yi, J.J. Won, K. Jeon, A. Yousef, R. Afeesh, M. El-Newehy, Photocatalytic activities of electrospun tin oxide doped titanium dioxide nanofibers. Ceram. Inter. **38**(6), 4533–4540 (2012)
42. A. Kadam, R. Dhabbe, D.S. Shin, K. Garadkar, K, & J. Park, Sunlight driven high photocatalytic activity of Sn doped N-TiO_2 nanoparticles synthesized by a microwave assisted method. Ceram. Inter. **43**(6), 5164–5172 (2017)
43. G. Sauthier, E. György, A. Figueras, R.S. Sánchez, J. Hernando, Laser Synthesis and Characterization of Nitrogen-Doped TiO_2 Vertically Aligned Columnar Array Photocatalysts. J. Phys. Chem. C **116**(27), 14534–14540 (2012)
44. M. Huimin Shi, D. Zhou, X.P. Song,Jiecai J. Fu, S. Zhou, T. Ma, Wang, Highly Porous SnO_2/TiO_2 Electrospun Nanofiberswith High Photocatalytic Activities, Ceram. Inter. 40(7), 10383–10393 (2014)
45. S. Prabakaran, K.D. Nishaa, J. Harish, M. Archana, S. Navaneethan, C. Ponnusamy, Y. Muthamizhchelvan, Hayakawa, Effect of Al doping on the electrical and optical properties of TiO_2 embedded Graphene Oxide nanosheets for opto-electronic applications. Appl. Surf. Sci **449**, 332–339 (2018)
46. M. Sun, W. Kong, Y. Zhao, X. Liu, J. Xuan, Y. Liu ,F.G. Jia, J. Yin, Wang, J. Zhang, Improving Photocatalytic Degradation Activity of Organic Pollutant by Sn^{4+} Doping of Anatase TiO_2 Hierarchical Nanospheres with Dominant {001} Facets, Nanomaterials 9, 1603 (2019)
47. G. Mathankumar, P. Bharathi, M. Krishna Mohan, S. Harish, M. Navaneethan, J. Archana, P. Suresh, G.K. Mani, P. Dhivya, S. Ponnusamy, C. Muthamizhchelvan, Synthesis and functional properties of nanostructured Gd-doped WO_3/TiO_2composites for sensing applications. Mater. Sci. Semicond. Process. **105**, 104732 (2020)
48. E. Freddy, B. Oropeza, R.G. Davies, Palgrave, R.G. Egdell, Electronic basis of visible region activity in high area Sn-doped rutileTiO_2 photocatalysts. Phys.Chem.Chem.Phys. **13**, 7882–7891 (2011)

49. G. Fu, Y. Yang, G. Wei, X. Shu, N. Qiao, L. Deng, Influence of Sn Doping on Phase Transformation and Crystallite Growth of TiO_2 Nanocrystals. J. Nanomaterials **835450**, 5 (2014) pages
50. R. Nadarajan, W. Azelee, W.A. Bakar, R. Ali, R. Ismail, Photocatalytic Degradation of 1,2-Dichlorobenzene using Immobilized TiO_2/ SnO_2/WO_3 Photocatalyst Under Visible Light: Application of Response Surface Methodology. Arab. J. Chem. **11**(1), 34–47 (2016)
51. A. Farhadi, M.R. Mohammadi, M. Ghorbani, On the assessment of photocatalytic activity and charge carrier mechanism of TiO_2@SnO_2 core-shell nanoparticles for water decontamination. J. Photochem. Photobiol. A **338**, 171–177 (2017)
52. S. Jiao, G. Lian, L. Jing, Z. Xu, Q. Wang, D. Cui, C.P. Wong, Sn-Doped Rutile TiO_2 Hollow Nanocrystals with Enhanced LithiumIon Batteries Performance, ACS Omega 3, 1329 – 1337 (2018)
53. Z. Xiufeng, L. Juan,L.Lianghai,and W. Zuoshan, Preparation of Crystalline Sn-Doped TiO_2 and Its Application inVisible-Light Photocatalysis. J. Nanomaterials **432947**, 5pages (2011)
54. S. Ghafoor, S. Ata, N. Mahmood, & S. N.Arshad, Photosensitization of TiO_2 nanofibers by Ag_2S with the synergistic effect of excess surface Ti^{3+} states for enhanced photocatalytic activity under simulated sunlight. Sci. Rep. (2017). DOI:10.1038/s41598-017-003667
55. S.R. Sanivarapu, J.B. Lawrence, G. Sreedhar, Role of Surface Oxygen Vacancies and Lanthanide Contraction Phenomenon of $Ln(OH)_3$(Ln = La, Pr, and Nd) in Sulfide-Mediated Photoelectrochemical Water Splitting, ACS Omega 3, 6267 – 6278 (2018)
56. S.M. Hassan, A.I. Ahmed, M.A. Mannaa, Preparation and characterization of SnO_2 doped TiO_2 nanoparticles: Effect of phase changes on the photocatalytic and catalytic activity. Journal of Science: Advanced Materials and Devices **4**, 400–412 (2019)
57. M. Zhou, J. Yu, S. Liu, P. Zhai, L. Jiang, Effects of calcination temperatures on photocatalytic activity of SnO_2/TiO_2 composite films prepared by an EPD method. J. Hazard. Mater. **154**, 1141–1148 (2008)
58. S. Amreetha, S. Dhanuskodi, A. Nithya, K. Jothivenkatachalam, Three Way Electron Transfer of C-N-S Tri Doped Two-Phase Junction of TiO_2 Nanoparticles for Efficient Visible Light Photocatalytic Dye Degradation, RSC Adv.(2016). DOI: 10.1039/C5RA25017J
59. D.P. Jaihindh, C.C. Chen, Y.P. Fu, Reduced graphene oxide-supported Ag-loaded Fedoped TiO_2 for the degradation mechanism of methylene blue and its electrochemical properties. RSC Adv. **8**, 6488 (2018)
60. T.Ali,P. Tripathi, AmeerAzam,W.R.A. SAhmed, A. Ahmed, M. Muneer, Photocatalytic performance of Fe-doped TiO_2 nanoparticles under visible-light irradiation, Mater. Res. Express. 4, 015022 (2017)
61. X. Li, R. Xiong, G. Wei, Preparation and photocatalytic activity of nanoglued Sn-doped TiO_2. J. Hazard. Mater. **164**, 587–591 (2009)
62. J. Du, G. Zhao, H. Pang, Y. Qian, H. Liu, D.J. Kang, A template method for synthesis of porous Sn-doped TiO_2 monolith and its enhanced photocatalytic activity. Mater. Lett. **93**, 419–422 (2013)
63. S.M. Hassan, A.I. Ahmed, M.A. Mannaa, Surface acidity, catalytic and photocatalytic activities of new type $H_3PW_{12}O_{40}$/Sn-TiO_2 nanoparticles. Colloids Surf. A **577**, 147–157 (2019)

64. F. Sayılkan, M. Asilturk, P. Tatar, N. Kiraz, E. Arpac¸, H. Sayılkan, Photocatalytic performance of Sn-doped TiO_2 nanostructured mono and double layer thin films for Malachite Green dye degradation under UV and vis-lights. J. Hazard. Mater. **144**, 140–146 (2007)
65. N. Karthikeyan, V. Narayanan, A. Stephen, Degradation of Textile Effluent using Nanocomposite TiO_2/SnO_2 Semiconductor Photocatalysts. Int.J. ChemTech Res. **8**(11), 443–449 (2015)
66. P.D. Bhange,, S.V. Awate, R.S. Gholap, G.S. .Gokavi, D.S.Bhange, Photocatalytic degradation of methyleneblue on Sn-doped titaniana noparticles synthesized by solution combustion route. Mater. Res. Bull. **76**, 264–272 (2016)
67. E.M. Bayan, T.G. Lupeiko, L.E. Pustovayayand, M.G. Volkova, Synthesis and photocatalytic properties of Sn–TiO_2 nanomaterials. Adv. Dielect **10**, 2060018 (2020)

Tables

Table .1 XRD parameters of Sn doped TiO_2 samples

Sample	2θ(in degree)	Phase	FWHM	Crystallite size(in nm)	D spacing (in nm)
ST1	27.87	Rutile	0.4624	18.5	0.3200
ST2	27.54	Rutile	0.6158	13.8	0.3236
ST3	27.14	Rutile	0.90994	9	0.3283
ST4	27.12	Rutile	0.8614	10	0.3285
ST5	27.08	Rutile	0.6296	13.6	0.3290

Table 2. Degradation rate constant for Sn doped TiO_2 nanomaterials

Sample	Rate constant (min^{-1})	R^2
ST1	0.04568	0.96017
ST2	0.0523	0.94493
ST3	0.0651	0.98868
ST4	0.04614	0.95903
ST5	0.05561	0.94808

Table 3. Comparison of different Sn doped TiO_2

S.No	Year	Author	Material	Morphology	Light Source	Dye	Irradiation Time (Min)	Degradation Percentage (%)
	2009	Y.F. Tu *et al. [15]*	Sn-doped TiO2	Nanotube	UV light	methylene blue	360 min	88 %
	2011	F.E. Oropeza *et al.[48]*	Sn-doped Rutile TiO2	spherical	Xe-light	methylene blue	360 min	65 %
	2011	Nadir Kiraz *et al[36]*	Sn doped nanometric TiO_2	spherical	UV light Visible light	malachite green malachite green	60 min 60 min	90 % 81 %
	2015	N.Karthikeyan *et al.*[65]	TiO_2/SnO_2 semiconductor nanocomposites	spherical	UV light	methylene blue	120 min	90 %
	2016	J.li *et al.[23]*	Sn-doped TiO2	Nanotube	Visible light Visible light	Rhodamine B nitrobenzene	100 min 300 min	94 % 92 %
	2016	P.D.Bhange *et al.[66]*	Sn-doped Titania	spherical	Visible light	methylene blue	300 min	90 %
	2018	S. Ehsan *et al. [39]*	Sn-doped TiO2	spherical	Sun light Visible light	methylene blue methylene blue	300 min 300 min	73% 50 %
	2019	C.M. Magdalane, *et al[36]*	SnO_2/TiO_2 nanostructure	spherical	Visible light	malachite green	75 min	96 %
	2020	E. M. Bayan et al.[67]	Sn–TiO_2 nanomaterials	spherical	UV light	methylene blue	120 min	77 %
	2020	**This work**	**Sn-doped TiO_2**	**spherical**	**Visible light**	**methylene blue**	**30 min**	**95.3 %**

Figures

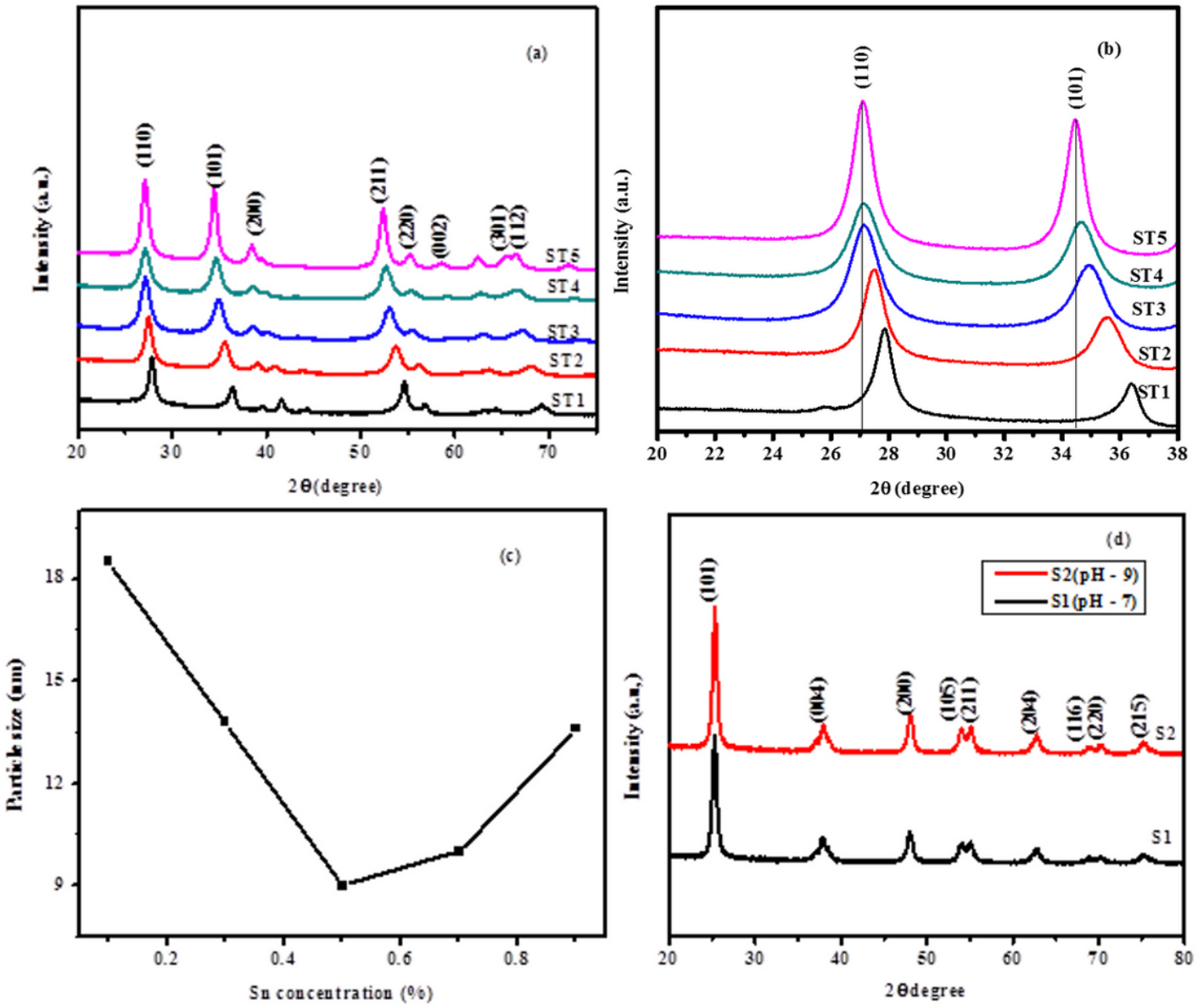

Figure 1

(a) XRD pattern of Sn doped TiO2 samples, (b) Extended view of XRD, (c) particle sizes for different concentration and (d) XRD pattern of TiO2 samples.

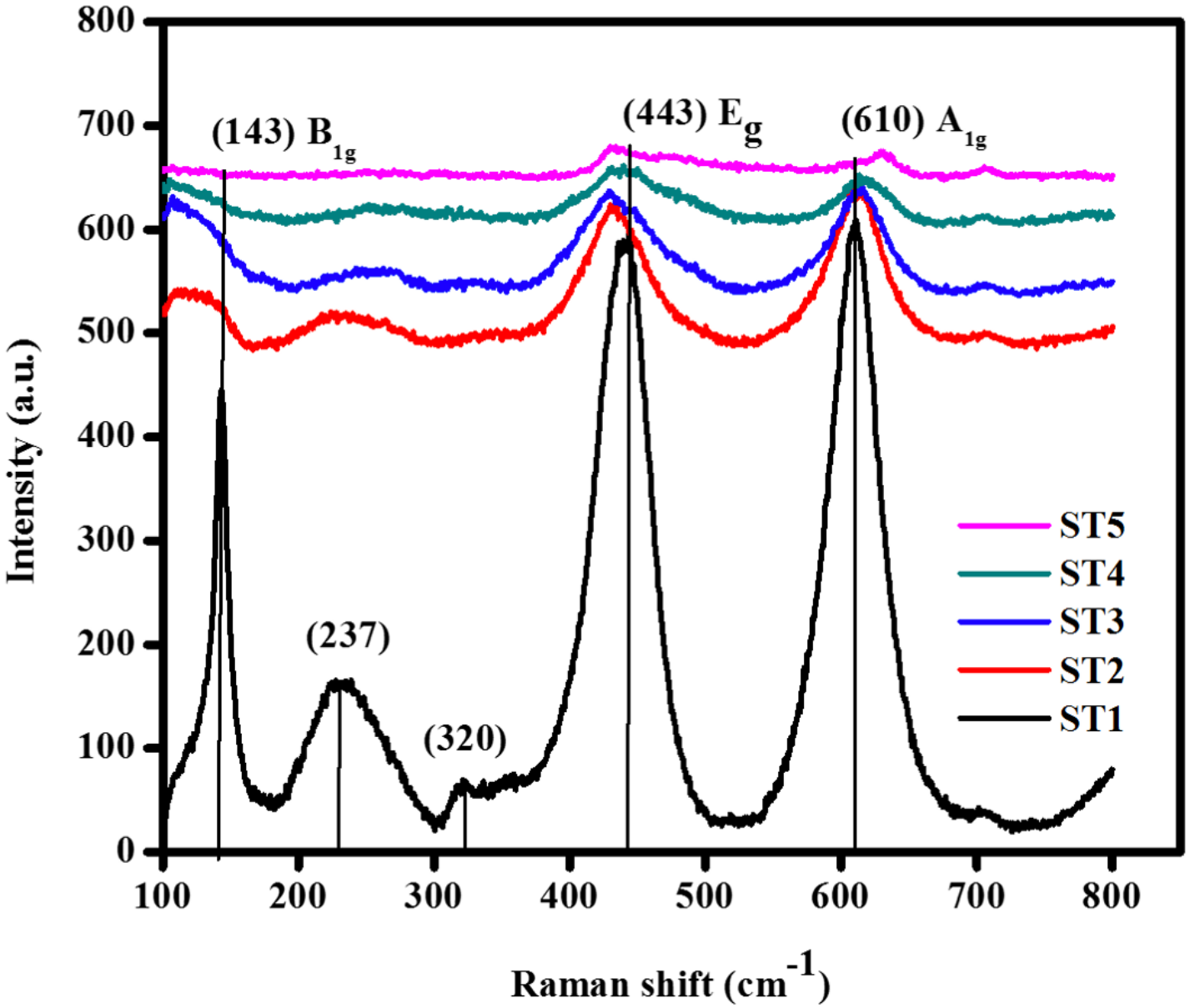

Figure 2

Raman spectra of Sn doped TiO2 nanoparticles.

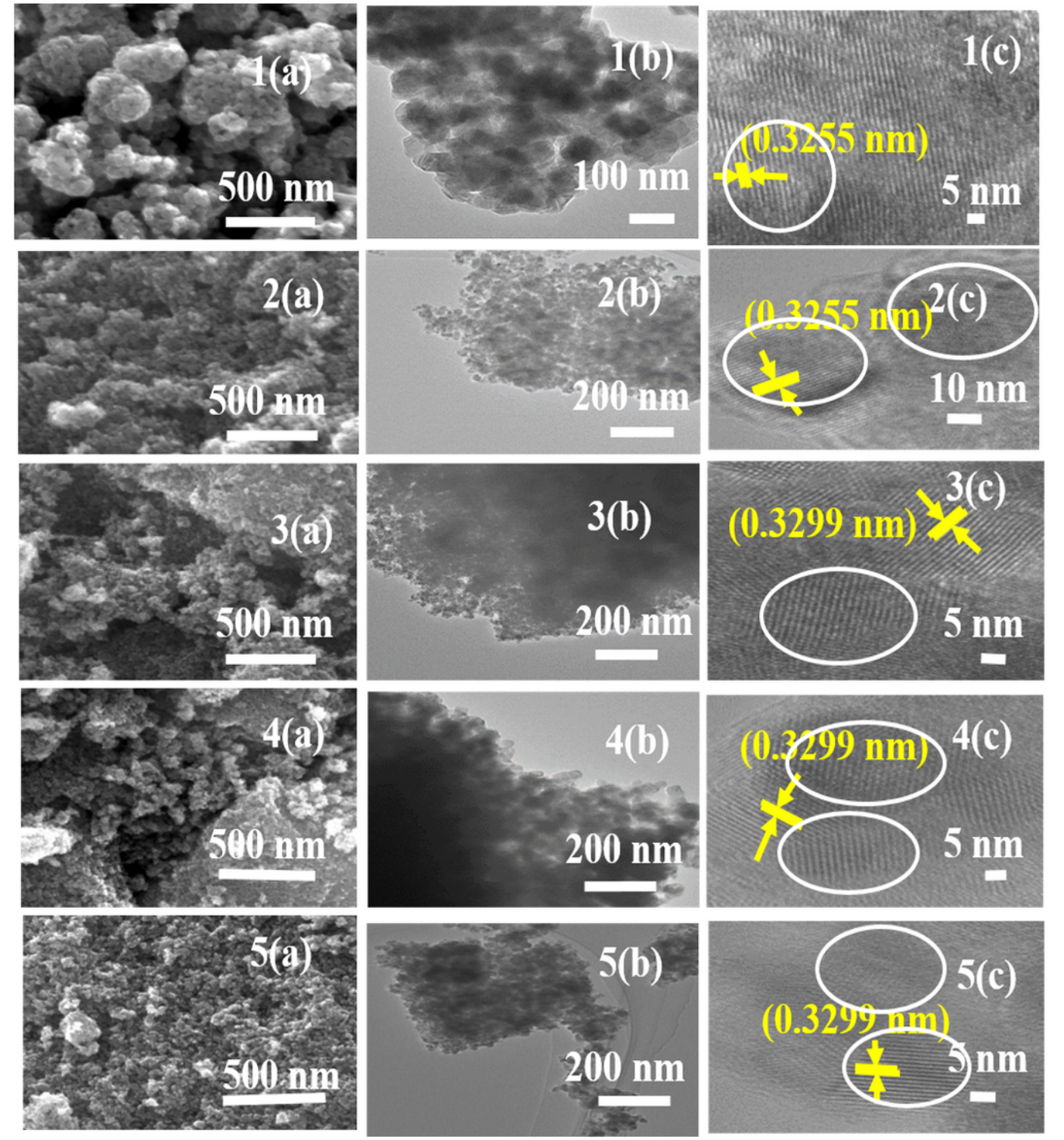

Figure 3

FESEM ,TEM and HRTEM images of ST1 [1 (a, b and c)], ST2 [2 (a, b and c)], ST3 [3 (a, b and c)], ST4 [4 (a, b and c)] and ST5 [5 (a, b and c)]

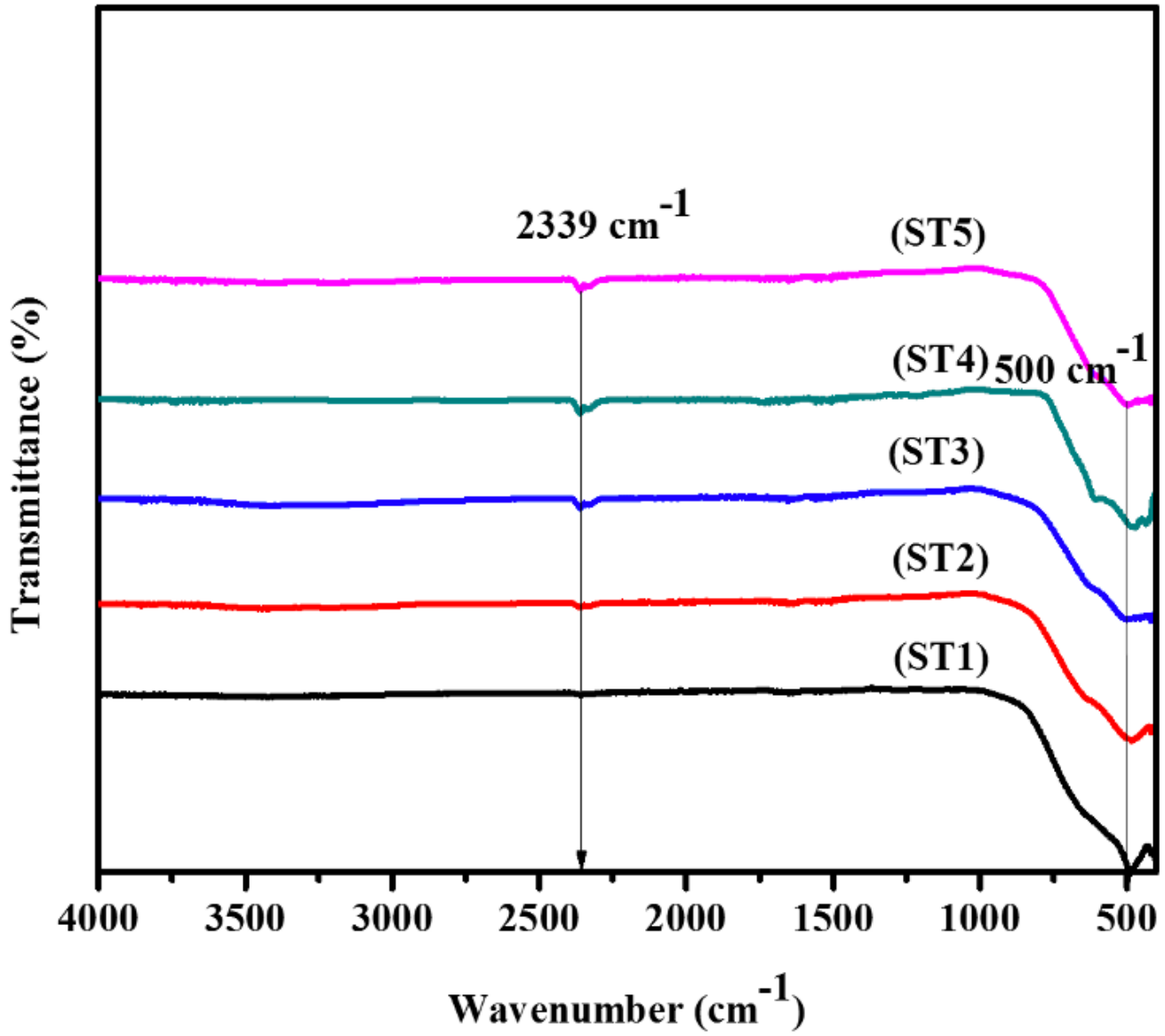

Figure 4

FTIR spectra of Sn doped TiO2

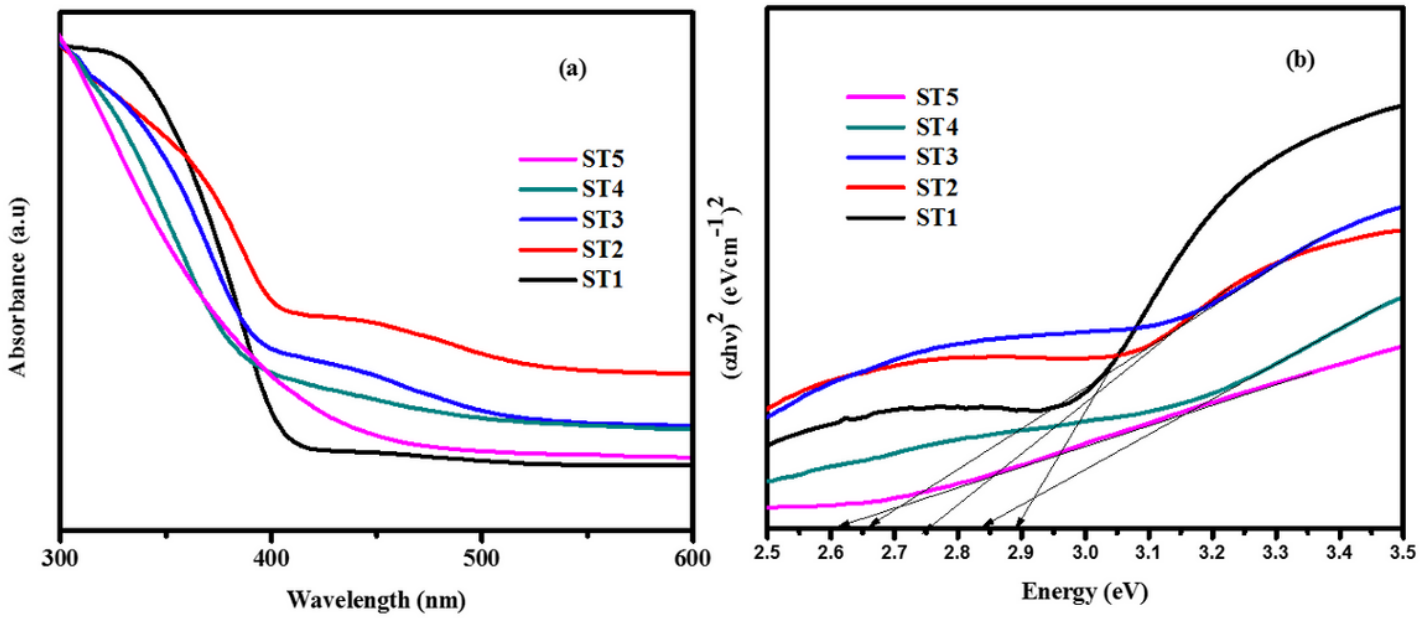

Figure 5

(a) UV – Vis diffuse absorbance spectra Sn doped TiO2 and (b) Tauc plot of Sn doped TiO2

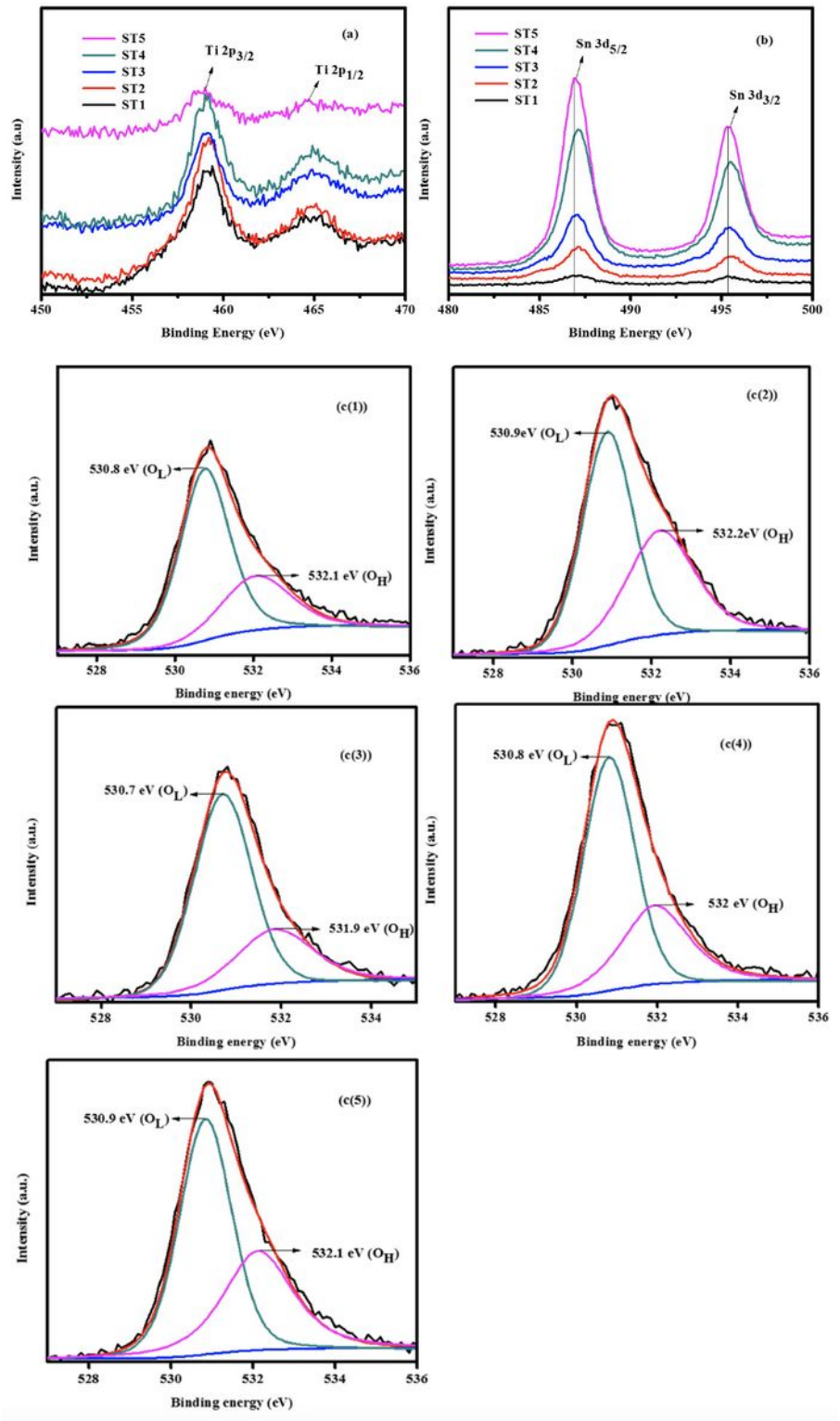

Figure 6

XPS analysis of Sn doped TiO2: (a) Ti 2p, (b) Sn 3d, (c) O1s

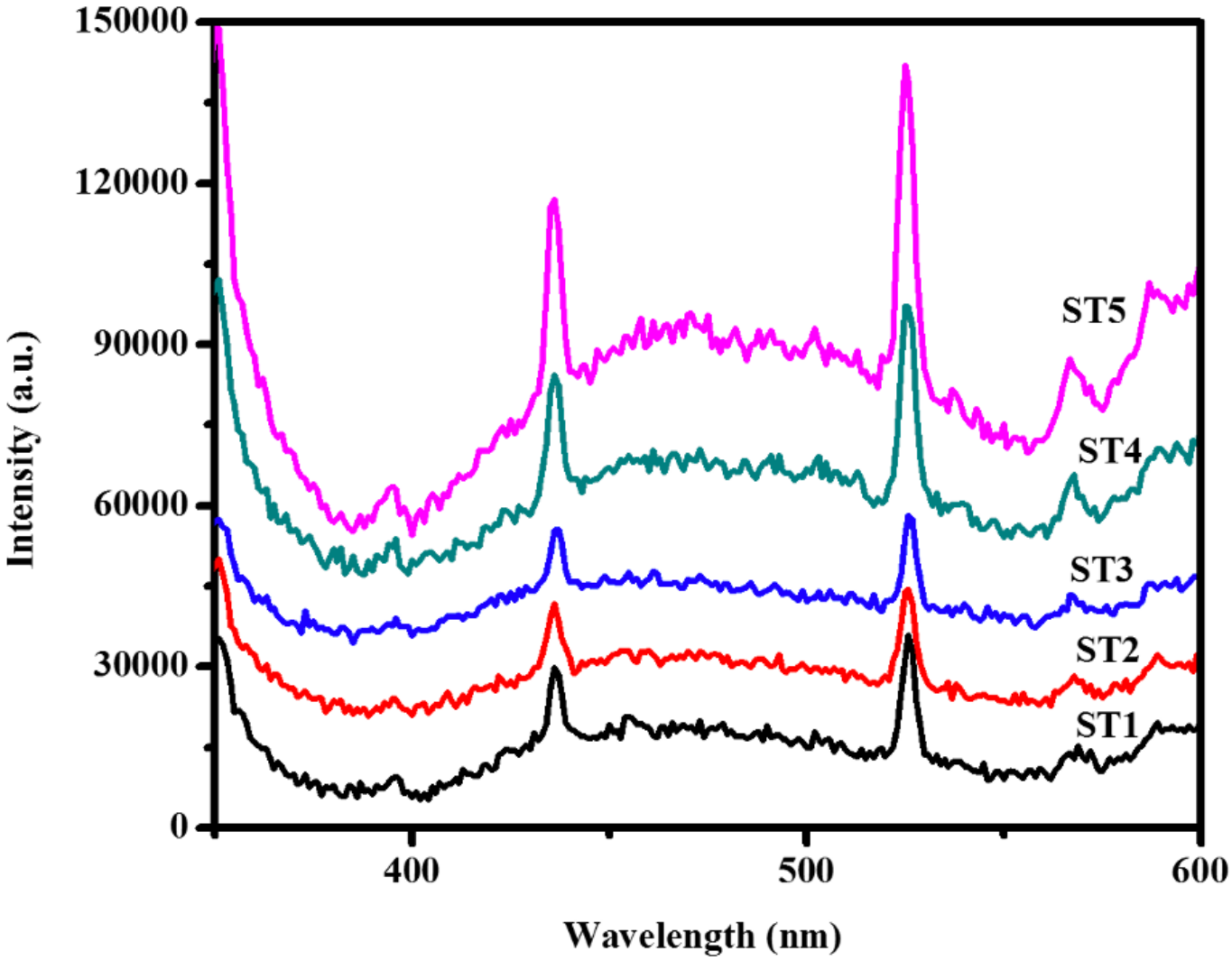

Figure 7

PL spectra of Sn doped TiO2

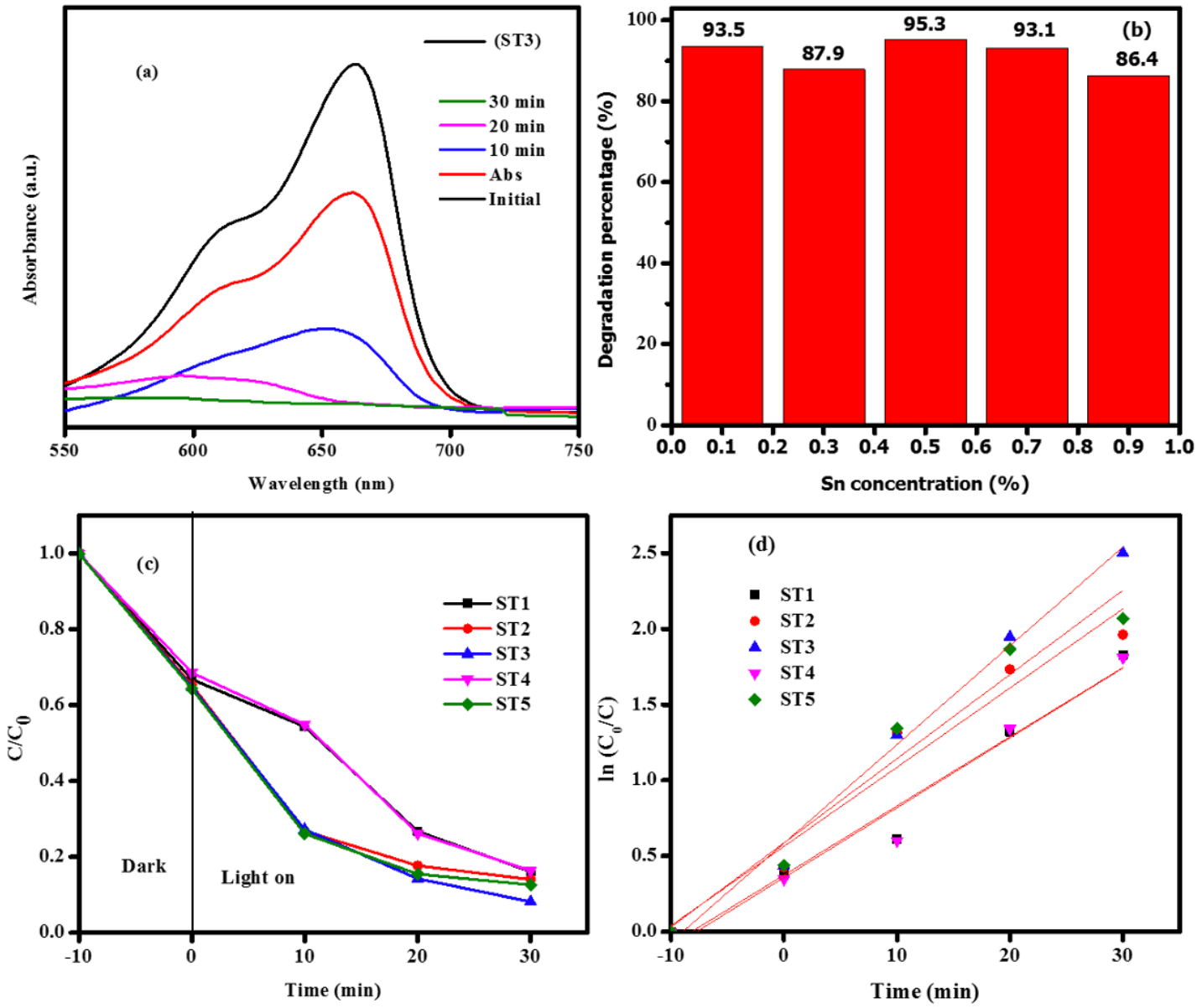

Figure 8

(a) Time-dependent UV-visible absorption spectra of the MB solution in the presence of ST3. (b) Different concentration of Sn on the photodegradation efficiency of MB under visible light. (c) photdegradation of MB solution for ST1 to ST5 photocatalyst. (d) kinetic curve for ST1 to ST5 photocatalyst..

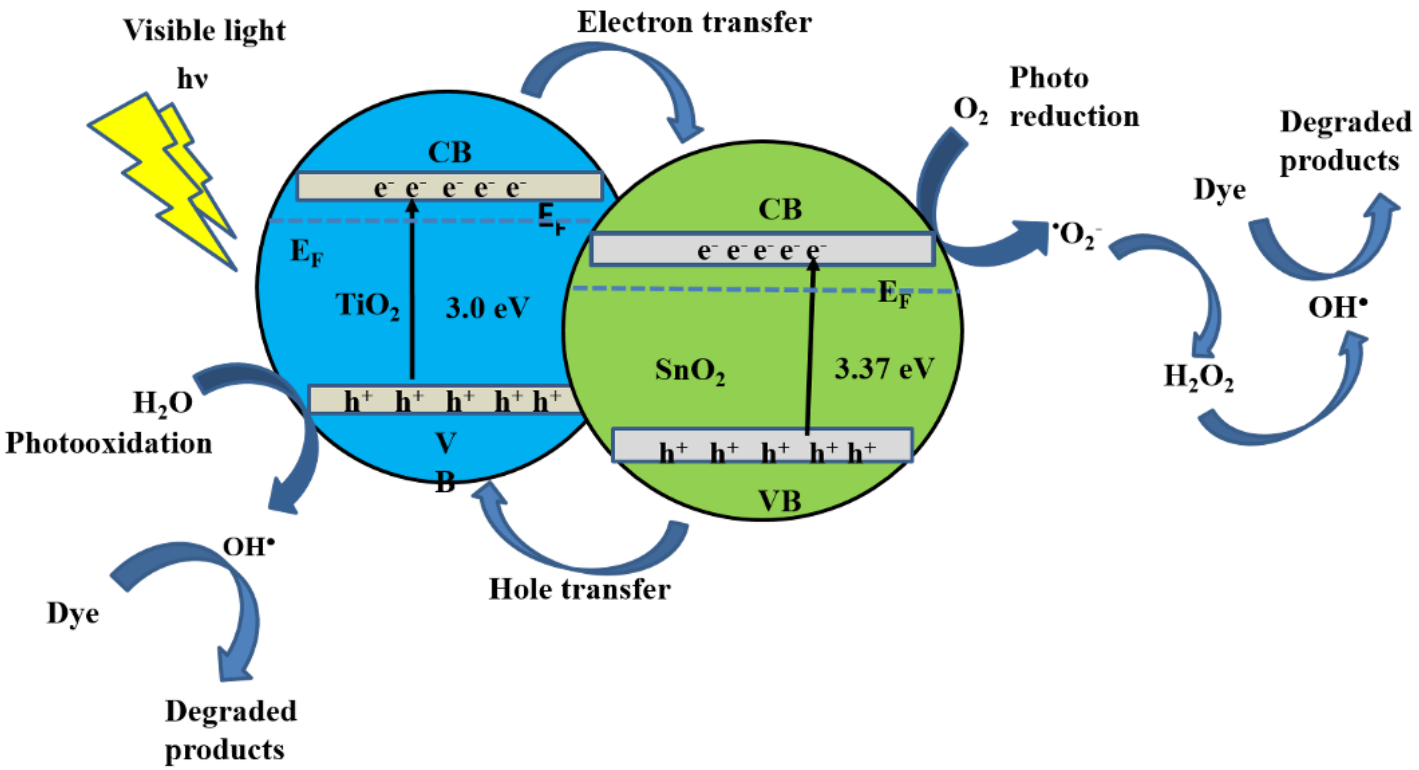

Figure 9

Mechanism of the MB degradation by using the Sn doped TiO2nanoparticles.

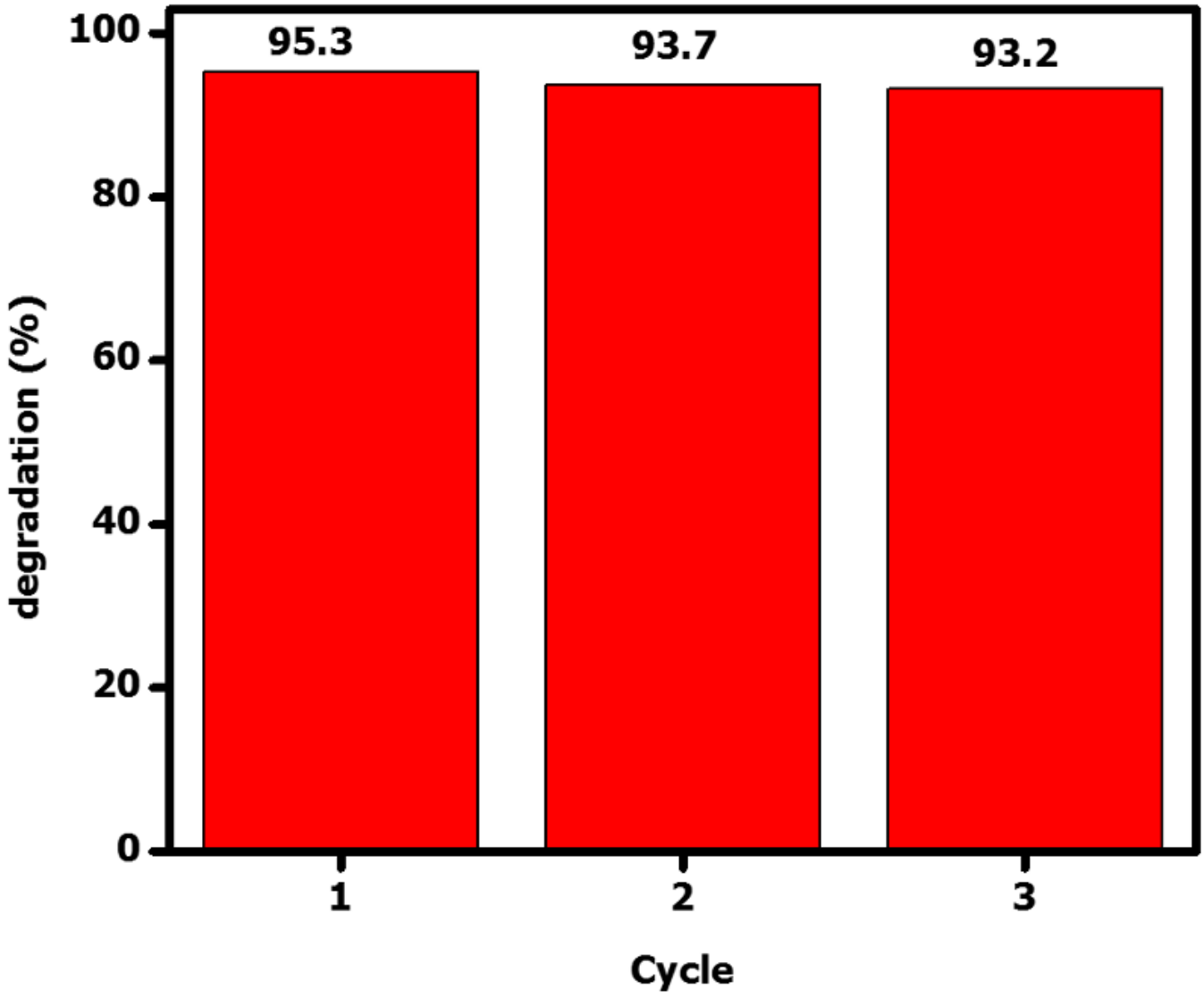

Figure 10

Reusability of MB solution for the ST3 sample under visible light irradiation.

Supplementary Files

This is a list of supplementary files associated with this preprint. Click to download.

- PatternI.png